Physics and Imaging in Radiation Oncology 12 (2019) 22–29

Contents lists available at ScienceDirect

Physics and Imaging in Radiation Oncology

journal homepage: www.elsevier.com/locate/phro

Original Research Article

A preferred patient decubitus positioning for magnetic resonance image guided online adaptive radiation therapy of pancreatic cancer

Yazheng Chen[a,b], Xinfeng Chen[a], William Hall[a], Phil Prior[a], Ying Zhang[a], Eric Paulson[a], Jinyi Lang[b], Beth Erickson[a], X. Allen Li[a,*]

[a] Department of Radiation Oncology, Medical College of Wisconsin, Milwaukee, WI, USA
[b] Sichuan Cancer Hospital & Institute, Radiation Oncology Key Laboratory Of Sichuan Province, Chengdu, China

ARTICLE INFO

Keywords:
Radiation therapy for pancreatic cancer
Decubitus positioning
Magnetic resonance image guided radiation therapy
Radiation dose escalation

ABSTRACT

Background and purpose: In radiotherapy (RT) for pancreatic cancer, the dose to adjacent organs-at-risk (OAR) often limits the delivery of curative dose. This work aimed to find a body decubitus position that would lead to increased separation between the duodenum and pancreatic head.

Materials and methods: Abdominal magnetic resonance images (MRI) of 11 healthy volunteers were acquired using a 1.5T MR-Linac for supine, left decubitus and right decubitus body positions. The geometry changes between different body positions were measured using Hausdorff Distance (HD) and overlap volume. RT plans were created on the MRIs. Commonly used dose-volume parameters (DVP), e.g., V_{40Gy} – volume received at least 40 Gy, for OARs were compared for the three body positions.

Results: The average of maximum HD between the duodenum and pancreatic head for all the cases was 4.0 ± 3.1 mm for supine, 7.3 ± 4.4 mm for left and 3.3 ± 1.4 mm for right positions ($P < 0.01$). The DVPs of the duodenum (e.g., V_{20Gy}, V_{45Gy}) for the left position were lower than those for the supine and right positions ($P < 0.01$). The right decubitus led to the highest duodenum DVPs. On average, the highest dose escalation was increased from 69 ± 4 Gy to 74 ± 5 Gy ($P = 0.002$) if body position was changed from supine to left decubitus.

Conclusion: The left decubitus increased the separation between duodenum and pancreas head, improving OAR sparing in RT for pancreatic cancer and allowing safer dose escalations to the tumor. The left decubitus positioning with proper immobilization could be adopted for MRI-guided adaptive RT.

1. Introduction

Pancreatic cancer (PC) is a fatal malignancy with an overall five-year survival rate of less than 5% despite aggressive combined modality treatment approaches [1–3]. Approximately 40% of PC patients present with locally advanced unresectable disease [4]. A subgroup of these patients who do not develop metastatic disease may be cured with advanced chemoradiation therapy (CRT) with high radiation doses [4].

Magnetic resonance image (MRI) guided RT (MRgRT) technology [5–7], such as integrated MRI scanner and linac (MR-Linac) or Co-60 machine, has recently been introduced into the clinic. Because of the superior soft tissue contrast from MRI and the capability of online adaptive replanning [8], MRgRT has been used for treating PC with substantially improved target coverage and/or organ at risk (OAR) sparing [9–13]. It has been shown that the radiation dose escalations with MRgRT significantly increased survival for a subset of PC patients [9]. However, as clearly demonstrated in recent studies [15,16], it is generally difficult to safely escalate radiation dose to the tumor due to the close proximity of OARs, particularly duodenum, to the pancreas in a large portion of the patient population, as most pancreatic tumors are located in the pancreatic head.

During RT, the patient is conventionally positioned supine. Due to gravity, the geometry of relevant organs can change with different body positioning. In particular, for RT of pancreatic cancer, the separation between the duodenum and the target (e.g., pancreas head) can change with different decubitus positions, supine, left, and right. The purpose of this work was to investigate whether there is a preferred positioning method that would lead to improved separation between the target and OARs, increasing the possibility of dose escalation for most of the suitable locally advanced PC patients in MRgRT.

* Corresponding author at: Department of Radiation Oncology, Medical College of Wisconsin, 8701 Watertown Plank Road, Milwaukee, WI 53226, United States.
E-mail address: ali@mcw.edu (X.A. Li).

https://doi.org/10.1016/j.phro.2019.11.001
Received 12 September 2019; Received in revised form 5 November 2019; Accepted 7 November 2019

2. Materials and methods

2.1. MRI data acquisition

MRI data from 11 healthy volunteers were acquired using a 1.5T MR-Linac system (Unity, Elekta AB) in three head-first body positions: supine, left decubitus and right decubitus under a research protocol appoved by the Institutional Review Board of the Medical College of Wisconsin. A photo showing the left decubitus positioning along with a simplified immobilization device is included in the Supplementary materials. For actual patient treatment, more complex immobilization may be used to improve patient comfortability and/or set-up reproducibility in decubitus positions. The imaging region covered a length starting above the diaphragm and extended inferiorly toward the lower poles of the kidneys. This scan length ensured all relevant structures for PC RT were included for RT treatment planning. Two of the 11 volunteers were also scanned with body positioned in 45° with respect to the left decubitus. A 3D T1 mDIXON sequence [14], which has a repetition time 6.7 ms, a flip angle of 15°, an acquired voxel size of 0.69 × 0.69 × 1.5 mm^3, the echo times of 2.2 ms and 4.9 ms, and bandwidth of 433.5 Hz/pixel, was used. All images were 3D gradient nonlinearity distortion corrected prior to use. The images covering from the diaphragm to the kidneys were acquired within 16 s with an expiratory breath hold. The field of view of the scan was 275 mm × 275 mm. Parallel imaging (SENSE, R = 2.5) with phase encoding in left–right direction was used. Coil sensitivity data were acquired for all the three different positions. All volunteers were instructed not to eat any food four hours before the scanning to mimic the situation for RT of PC.

2.2. Geometric impact of decubitus position

The MRI data were transferred to a research planning system (Monaco v5.19.03d, Elekta, AB), where organs such as the stomach, duodenum, large bowel, small bowel, kidneys and spinal cord, along with the pancreatic head were delineated separately for each body position without an image registration. To mimic most clinical situations where gross tumor volume (GTV) is within the pancreatic head, we defined the GTV as the pancreatic head minus 5 mm isotropically and the planning target volume (PTV) as the GTV plus a 5 mm uniform margin, happening to be the pancreatic head. This represents an idealized scenario where there is no tumor invasion to the duodenum or surrounding structures.

To quantify geometrical characteristics of different body positions, Hausdorff distance (HD) [15], overlap volume (OV) and relative OV (ROV) were calculated between PTV and duodenum using an in-house Matlab program. The HD was defined as a minimum distance between any points from the two contours in a slice-by-slice fashion. The mean and maximum HD across all slices (HD_{mean} and HD_{max}) were compared among different decubitus positions. To evaluate the closeness of two organs in a 3D basis, four outer shells of different distance (5, 10,15 and 20 mm) from the duodenum were created around pancreatic head contours. The ROV was then defined as the volume of the overlap between an outer shell and the duodenum divided by the duodenum volume.

2.3. Dosimetric impact of different body position

Dosimetric plans were created on MRI with bulk electron density assignment for MR-Linac [16–18]. The research Monaco planning system is embedded with Graphics Processing Unit based Monte Carlo dose engine (GPUMCD, Elekta AB) that can compute dose in the presence of a transverse 1.5T magnetic field. All plans were calculated with the 7 MV flattening filter free (FFF) beam model using 0.3 cm grid spacing and 1% statistical uncertainty. Two sets of plans were generated for each decubitus position of each volunteer: five beam step-and-shoot intensity modulated RT (IMRT) and volumetric-modulated arc therapy (VMAT) plans based on the same dose prescription of 50.4 Gy in 28 fractions to the PTV and the same dose volume criteria commonly used in our clinic for pre-operative RT of resectable PC. Examples of these criteria include: the dose to 95% of PTV (D_{95}) ≥ 50.4 Gy; the maximum dose (D_{max}) ≤ 45 Gy for spinal cord; Dmax ≤ 53 Gy for duodenum; the volume irradiated by at least 45 Gy (V_{45Gy}) ≤ 25% and D_{max} ≤ 53 Gy for the bowels (small & large) and stomach, and V_{30Gy} ≤ 30% and the mean dose (D_{mean}) ≤ 28 Gy for liver, V_{15Gy} ≤ 25% for the kidneys. The beam angles used for IMRT were configured as 280°, 325°, 35°, 80°and 160° for the supine, 255°, 170°, 125°, 55° and 10° for the left, and 70°, 350°, 305°, 235°and 190° for the right positions. These configurations allow beam angles to rotate synchronously with decubitus change, minimizing the dosimetric effect from different beam angles. Dosimetric differences between the types of plans were compared to determine optimal decubitus position.

As VMAT generally leads to high dose gradients, VMAT dose escalation plans were generated to determine the maximally possible prescription dose to GTV (GTV D_{95} ≥ 100% of the prescription dose) that maintains acceptable OAR dose-volume criteria, e.g., D_{max} ≤ 45 Gy for the spinal cord, V_{45Gy} ≤ 25%, V_{56Gy} ≤ 5 cc and D_{max} ≤ 61 Gy for the stomach, V_{56Gy} ≤ 5 cc and D_{max} ≤ 61 Gy for the duodenum, V_{30Gy} ≤ 30% and D_{mean} ≤ 28 Gy for the liver, V_{45Gy} ≤ 25% and D_{max} ≤ 61 Gy for the bowels, and V_{15Gy} ≤ 25% for the kidneys. To further spare the kidneys, VMAT arcs were set as: 350°∼180° (Clockwise, 2 arcs) plus 260°∼290°(Clockwise) for left decubitus plans, 240°∼120° (Clockwise, 2 arcs) for supine decubitus plans. The dose escalation plans generated for the supine and the optimal position for each case were compared. Note that VMAT, not available with MR-Linac currently, is a future delivery model in MRgRT.

2.4. Data statistical method

Statistical analysis was carried out using the Statistical Package for Social Science (SPSS version 25.0, IBM, Chicago). Comparisons of geometric changes and dose-volume parameters between the three decubitus positions were performed. *Paired t*-test was used for both samples with a normal distribution determined by plotting the data in a histogram with normal curve, and Wilcoxon signed-rank test for related samples was used when any sample among the pair deviated from the normal distribution. Statistical significance was defined as a *P*-value with a value of less than 5% significance (i.e. $P < 0.05$). Pearson product-moment correlation coefficients were used to determine the correlation between the geometric parameters (e.g., HD_{mean}, HD_{max}, and ROVs of different outer shells between pancreatic head and duodenum) and the dosimetric parameters (e.g, V_{45Gy}, V_{30Gy}, V_{20Gy}, D_{mean}, and D_{max} of duodenum). The linear regression model was used to analyze the correlation.

3. Results

3.1. Geometric improvements

Fig. 1 shows MRIs of different decubitus positions (supine, left, right, 45°) for an extreme case, where the HD_{max} value between the duodenum and pancreatic head was 14.6 mm for supine, 18.1 mm for left, 4.7 mm for right, and 7.1 mm for 45° positions, as indicated in the figure. The HD_{mean} values, along with other data, for all cases are compared between the supine and left positions in Table 1. For all case studies, the left decubitus led to increased separation between pancreatic head and duodenum with larger HD_{mean} (3.1 ± 0.8 mm, $P = 0.0001$, t = 5.9) and HD_{max} (7.3 ± 4.4 mm, $P = 0.001$, t = 4.5), compared with both supine (HD_{mean} = 1.5 ± 0.5 mm and HD_{max} = 4.0 ± 3.1 mm) and right positions (HD_{mean} = 1.2 ± 0.2 mm and HD_{max} = 3.3 ± 1.4 mm). The largest increase was 17.3 mm when body position changed from supine to left.

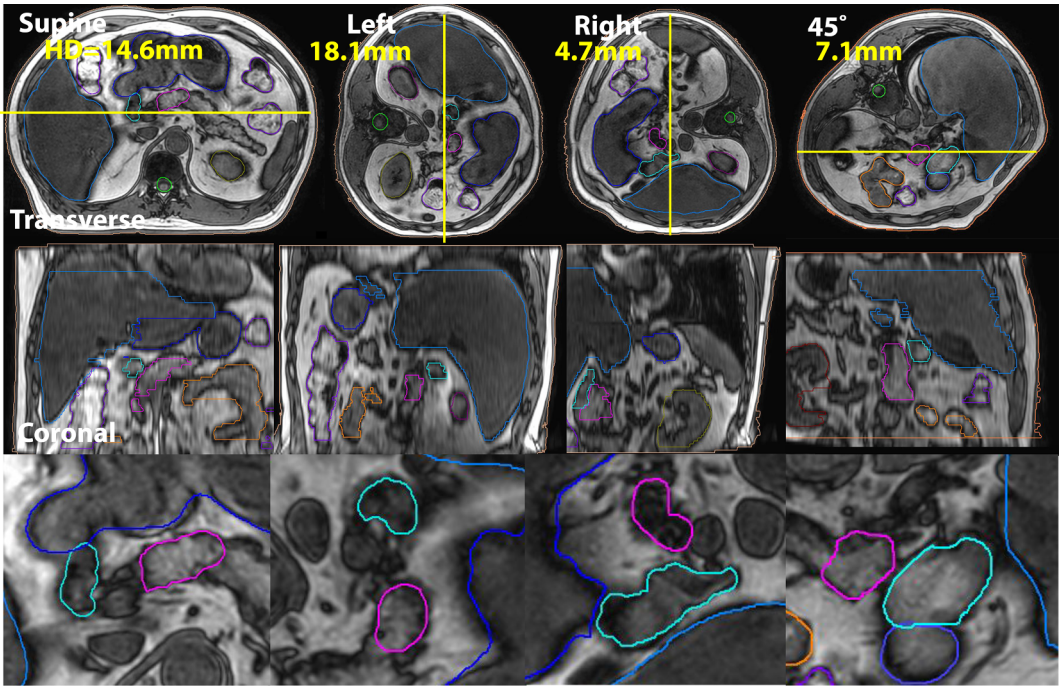

Fig. 1. An axial (top), coronal (middle) and zoomed axial (bottom) views of T1 MRI for the supine, left, right and 45° decubitus positions of an extreme case. The coronal plane was indicated as the yellow line on the axial plane for each decubitus. The Hausdorff Distance (HD) between the pancreatic head and duodenum are included. Contours of pancreas head (pink), duodenum (turquoise), spinal cord (bright green), stomach (blue), liver (light blue), large bowel (bluish violet), and small bowel (light orange) are shown. (For interpretation of the references to colour in this figure legend, the reader is referred to the web version of this article.)

For all cases in left position, the ROVs were significantly smaller than those for both supine and right positions. The mean OV values for 1 cm shell derived from 11 volunteers in both supine and left decubitus were13.9 ± 4.0 and 10.8 ± 3.1 cm^3, respectively, indicating less overlap volumes with left position ($P = 0.003$, t = 4.0). The geometric improvements for the 45° position were worse than those for the left position and, thus, are not presented. More detailed geometric parameters and data can be found in the Supplementary Materials.

3.2. Dosimetric gains

The dose distribution and dose volume histogram (DVH), along with selected DVH parameters for PTV and selected OARs of a representative case, are shown in Fig. 2 and Table 2. It is clear that the DVHs of the duodenum are different among the three decubitus positions (Table 2). For example, the D_{mean} of the duodenum with the left position was 26 Gy, reduced by 17% and 34%, respectively, from those for the

Table 1
A comparison of selective dosimetry and geometry parameters of duodenum between the supine and left decubitus for the 11 cases. The values of HD_{mean}, HD_{max}, Overlap Volume(OV), V_{20Gy}, V_{45Gy}, D_{1cc}, D_{5cc}, and the safe dose escalation (DE) are included.

Duodenum		HD_{Mean}/mm	HD_{max}/mm	OV (cm^3)	V_{20Gy} (%)	V_{45Gy} (%)	D_{mean}(Gy)	D_{1cc}(Gy)	D_{5cc}(Gy)	DE(Gy)
1	Supine	2.2	11.5	11.2	72.5	19.5	30.7	50.0	43.3	65
	Left	4.3	13.6	7.3	62.3	10.0	26.2	49.5	38.7	74
2	Supine	1.3	2.3	19.2	96.3	17.5	33.9	50.5	46.9	69
	Left	3.0	5.9	12.7	73.2	5.6	27.2	47.6	40.4	80
3	Supine	1.5	4.0	20.3	96.7	22.9	35.8	49.9	47.4	73
	Left	3.7	8.2	11.2	63.3	7.8	26.7	48.5	42.9	84
4	Supine	1.3	2.7	10.3	72.1	15.3	29.1	49.8	45.5	77
	Left	2.3	3.4	9.7	71.2	12.5	27.1	49.8	43.4	79
5	Supine	1.3	2.1	9.5	87.6	23.1	34.4	50.3	43.1	65
	Left	1.6	3.1	10.3	53.0	5.8	25.5	45.9	35.0	70
6	Supine	1.0	2.1	11.6	83.9	20.1	33.1	49.9	40.5	66
	Left	3.5	6.4	6.8	59.4	9.4	26.3	47.0	31.4	68
7	Supine	2.1	3.8	9.1	70.1	10.1	27.6	48.0	37.7	70
	Left	3.2	7.5	7.9	48.7	6.9	24.5	46.3	34.9	75
8	Supine	0.9	1.5	12.4	78.2	17.5	31.5	49.7	43.1	70
	Left	2.3	4.6	11.5	73.7	11.6	29.4	48.3	39.5	69
9	Supine	1.0	2.3	14.8	72.9	16.6	30.8	49.3	42.3	62
	Left	2.9	4.4	10.0	69.2	11.2	28.6	48.2	38.8	69
10	Supine	2.0	8.2	15.4	61.0	10.9	25.4	49.7	42.6	73
	Left	4.2	17.3	14.4	49.4	7.0	22.2	47.6	39.8	74
11	Supine	1.7	3.0	18.6	71.7	12.9	29.3	49.6	44.3	73
	Left	2.9	5.5	17.2	69.6	8.7	28.4	48.2	43.1	76
	P	0.000	0.001	0.003	0.002	0.000	0.000	0.001	0.000	0.002
	t	5.939	4.520	3.973	4.107	5.374	5.130	4.918	5.869	4.070
Average	Supine	1.5 ± 0.5	4.0 ± 3.1	13.9 ± 4.0	78.7 ± 11.4	16.6 ± 4.5	31.1 ± 3.1	49.7 ± 0.7	43.3 ± 2.7	69.4 ± 4.5
	Left	3.1 ± 0.8	7.3 ± 4.4	10.8 ± 3.1	63.5 ± 10.0	0.25 ± 2.18	25.6 ± 2.0	47.9 ± 1.2	38.9 ± 43.8	74.4 ± 5.2

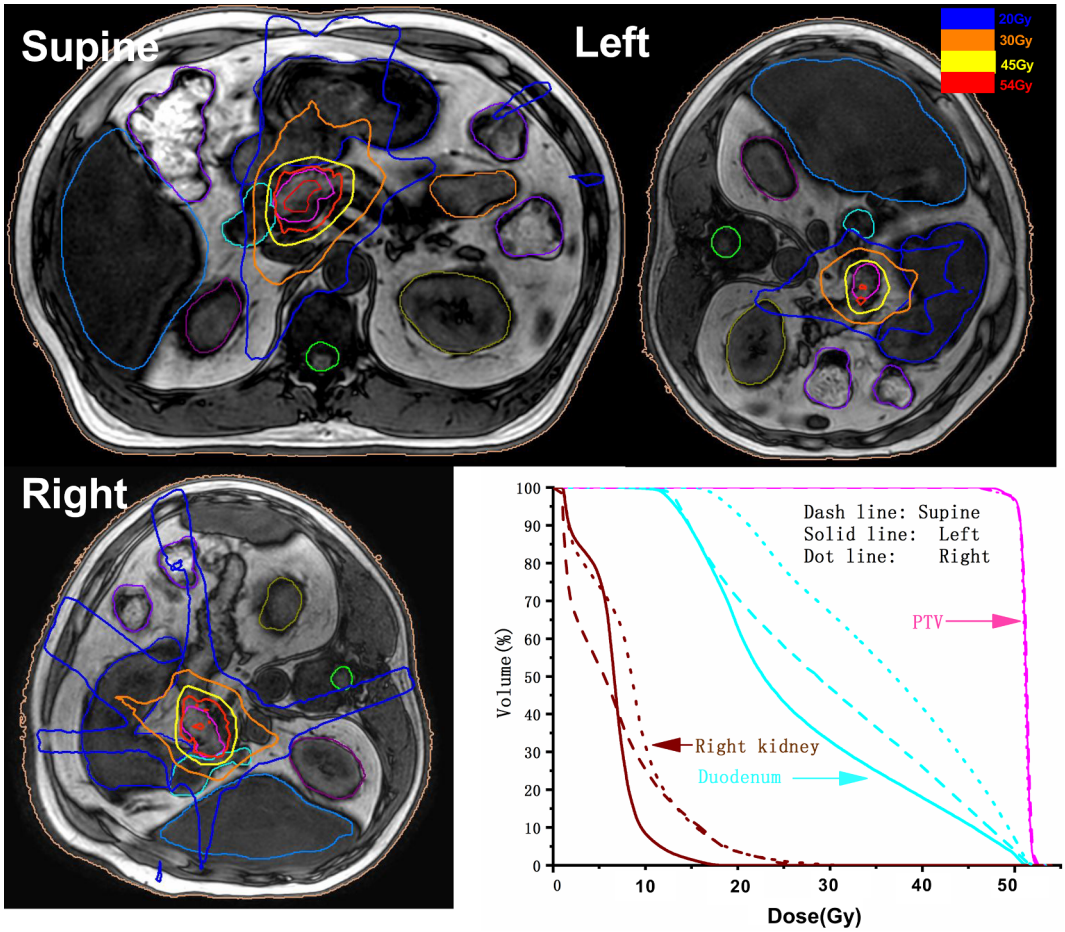

Fig. 2. The comparison of dosimetry data for the supine, left and right decubitus positions of a representative case. Dose distributions at an axial plans and dose volume histograms are compared.

supine (30 Gy) and right decubitus (35 Gy). The V_{20Gy}, V_{30Gy}, V_{45Gy} also show the similar trend. For other OARs (bowels, stomach, liver, kidneys), there was no clear trend, although the V_{45Gy} for the large bowel, small bowel and stomach and V_{30Gy} for the liver approximated to zero with the left position. For this reason, the detailed data for these OARs are not presented.

Key dosimetry parameters of duodenum for the left and supine positions are compared in Table 1 for all 11 cases. The increased separation between duodenum and pancreatic head with the left decubitus can be reflected by the dosimetry gains. For example, the duodenum V_{20Gy} for the left decubitus were reduced by as much as 35%, with mean ± standard deviation (SD) reduced from 78.7 ± 11.7 to 63.5 ± 10.0 from the supine to the left decubitus ($P = 0.002$, t = 4.1). The V_{45Gy} values reduced by 19% to 75%, with the mean and SD from 16 ± 4 to 9 ± 2 ($P < 0.001$, t = 5.4) from the supine to the left positions. Mean dose D_{mean} decreased by 3% to 25%, with mean and SD from 25 ± 2 to 31 ± 3 Gy ($P < 0.001$, t = 5.3). D_{5cc} reduced by 3% to 23%, with mean and SD from 43 ± 3 to 39 ± 4 Gy ($P < 0.001$, t = 5.9). The average dose escalations to the GTV can reach 74 ± 5 Gy for the left position versus 69 ± 5 Gy for the supine position ($P = 0.002$, t = 4.0). The dose escalation can reach as high as 80 Gy with the left postion, comparing to 69 Gy with the supine position for the same volunteer. The data for the right decubitus were generally worse than those for the left and supine positions, thus, are excluded in Table 1.

Fig. 3 compares selected duodenum DVH parameters of the three positions for all cases. It can be seen from Fig. 3(a), (b), (c) and (d) that the data points of the selected DVPs for the left decubitus locate at the lowest levels. The mean and SD of V_{20Gy}, V_{30Gy}, V_{45Gy}, D_{mean}, and D_{5cc} of the three decubitus positions are compared in Fig. 3(e). These data imply the advantages of the left position over the other two decubitus positions. The right decubitus is the worst among the three positions. More detailed data can be found in the Supplementary Materials.

3.3. Correlation of geometry and dosimetry

The dosimetric gains from supine to left decubitus positions were found to be correlated with the geometric improvements. The Pearson product-moment correlation coefficients for four pairs of parameters of ROV_{10mm} vs V_{45Gy}, HD_{mean} vs D_{mean}, ROV_{10mm} vs V_{30Gy}, and ROV_{10mm} vs D_{mean} were 0.73, −0.71, 0.69 and 0.66, respectively. The linear formulas, $Y = a*X + b$, where a and b are regression constants, Y is a dosimetric parameter and X is a geometric parameter, was used to fit the available data. The linear fits, as well as the 95% confidence, intervals are shown in Fig. 4. The obtained formula and Adjust R^2 value were also included in the figure.

4. Discussion

Although patients are normally setup in the supine position during RT delivery, alternate positions, such as the prone position for breast irradiation [22–24], are used to improve geometry, patient comfortability, and/or reproducibility. This study aimed to find a superior decubitus position for RT of pancreatic cancer, where the delivery of

Table 2
Comparison of selected dosimetry parameters at the supine, left and right body positions for a representative case.

	PTV(% or Gy)				Duodenum (Gy)		LB(Gy)	SB(Gy)	Stomach (Gy)	Liver (Gy)	LK(Gy)	RK(Gy)
	$V_{90\%}$	$V_{95\%}$	$D_{98\%}$	$D_{02\%}$	D_{mean}	D_{1cc}	D_{max}	D_{max}	D_{max}	D_{mean}	V_{15Gy}	V_{15Gy}
Supine	99.94	98.97	49.78	52.22	30.65	50.04	28.23	36.49	49.20	3.48	1.21	17.54
Left	100.00	99.75	49.26	52.02	26.20	49.45	33.91	40.81	35.28	7.15	18.6	18.29
Right	99.99	98.97	49.83	52.08	35.10	50.41	44.59	37.71	45.37	6.36	4.43	5.36

Duodenum		HD_{Mean}/mm	HD_{max}/mm	1cm overlap (cm^3)	V_{20Gy}(%)	V_{45Gy}(%)	D_{mean}(Gy)	D_{1cc}(Gy)	D_{5cc}(Gy)	Dose escalation (Gy)
1	Supine	2.02	11.52	11.19	72.52	19.47	30.65	50.04	43.34	65
	Left	3.19	13.57	7.28	62.30	10.00	26.20	49.46	38.72	74
2	Supine	2.17	7.50	19.20	96.30	17.46	33.99	50.54	46.85	69
	Left	3.44	7.50	12.66	73.57	5.59	27.21	47.62	40.37	80
3	Supine	2.30	6.85	20.26	96.65	22.92	35.84	49.86	47.38	73
	Left	3.09	8.17	11.21	63.33	7.83	26.72	48.53	42.93	84
4	Supine	1.41	2.81	10.33	72.13	15.34	29.14	49.81	45.53	77
	Left	2.32	3.41	9.73	71.23	12.51	27.08	49.76	43.44	79
5	Supine	1.43	2.37	9.46	87.6	23.07	34.36	50.31	43.12	65
	Left	1.60	3.09	7.41	53.00	5.78	25.52	45.89	34.99	70
6	Supine	1.03	2.08	11.63	83.89	20.12	33.12	49.89	40.54	66
	Left	3.41	6.36	6.82	59.35	9.35	26.33	47.02	31.40	68
7	Supine	1.83	3.75	9.08	70.06	10.12	27.62	47.98	37.73	70
	Left	2.45	7.50	7.93	48.74	6.94	24.50	46.34	34.92	75
8	Supine	1.24	2.77	12.41	78.15	17.46	31.52	49.70	43.05	70
	Left	2.15	4.62	11.48	73.69	11.60	29.40	48.32	39.49	69
9	Supine	1.28	3.00	14.84	72.89	16.6	30.76	49.34	42.29	62
	Left	2.52	4.40	10.01	69.21	11.25	28.57	48.21	38.79	69
10	Supine	3.02	19.25	13.30	61.01	10.9	25.37	49.74	42.61	73
	Left	3.54	20.41	12.24	49.41	7.03	22.19	47.62	39.79	74
11	Supine	1.72	3.00	18.59	71.69	12.89	29.28	49.64	44.25	73
	Left	2.94	5.53	17.16	69.6	8.66	28.44	48.17	43.05	76
Average	Supine	1.77 ± 0.58	5.90 ± 5.30	13.66 ± 4.02	78.66 ± 11.37	16.55 ± 4.52	31.06 ± 3.13	49.71 ± 0.66	43.33 ± 2.74	69.36 ± 4.50
	Left	2.78 ± 0.62	7.69 ± 5.13	10.45 ± 3.14	63.47 ± 10.00	9.25 ± 2.18	25.56 ± 2.02	47.90 ± 1.18	38.90 ± 43.80	74.36 ± 5.16

PTV: Planning Target Volume. LB: Large bowel, SB: Small Bowel, LK: Left Kidney, RK: Right Kidney. $V_{90\%}$, $V_{95\%}$: percentage of PTV receiving ≥90%,99% of the dose prescription, respectively; $D_{98\%}$,$D_{02\%}$: minimum dose (Gy) covering 98%, 2% of the PTV; V_{15Gy}: relative volume of the organs receiving ≥15 Gy; D1cc: dose of 1 cc volume; D_{max}, Dmean: maximum and mean dose (Gy).

curative RT dose may be prohibited due to the close proximity of OARs (e.g., duodenum, bowels, stomach). The data indicate that the left decubitus results in significantly improved geometry and dosimetry compared to those for the supine and right decubitus ($P < 0.05$). Data of right decubitus is the worst compared with supine and left decubitus ($P < 0.05$). Due to the geometric relationship between the duodenum and pancreas, we do not anticipate the separation between the two organs will be practically different for prone versus supine positioning. Thus, the prone position was not investigated in the study.

For the cases studied, the average HD_{max} between the duodenum and pancreatic head were 4.0 ± 3.1 mm, 7.3 ± 4.4 mm, 3.3 ± 1.4 mm for the supine, left and right decubitus, respectively. The duodenum, which is connected to distal stomach, was separated more from pancreas head in the left decubitus as compared to other body positions. The overlap volume data show $OV_{left} < OV_{supine} < OV_{right}$ ($P < 0.001$). The less overlap between pancreas head and duodenum led to reduced dose to the duodenum, providing the possibility of higher dose escalation as compared to the supine and right decubitus.

Feng et al has proposed to use biodegradable hydrogel spacer that is injected between duodenum and pancreas head [18]. This method, although effective to separate the duodenum and pancreas, is invasive. The authors proposed an overlap volume histogram model to predict which patient requires the placement of a hydrogel spacer. Based on the present data, we established a relationship between the geometry improvement and the dosimetry gain, allowing to estimate dose volume changes from the geometric parameters in practical settings.

It has been reported that radiation dose escalation improves treatment outcome of RT for locally advanced pancreatic cancer [19–22]. It is desirable to escalate the dose to above 70 Gy in 2 Gy fractions [22,23]. However, safe dose escalation to this dose level is often limited by the dose constraints of adjacent OARs. Our study indicates that the increased separation between the pancreatic head and duodenum in left decubitus are helpful to achieve the dose escalation. For the cases studied, the dose to the GTV can be escalated as high as 80 Gy without violating the OAR dose constraints for the left decubitus position. These dosimetric data, although generated for conventional fractionation, can be scaled for other fractionations (e.g., SBRT).

There are several limitations in this study. Though the significant trend is detected among three body positioning methods, a larger sample size may help to confirm the findings. The bulk electron density assignment was used during MRI-based planning, which can introduce dosimetry uncertainty as compared with the computerized tomography (CT) based planning. As the online replanning time is generally long, the intrafraction motions between the decubitus positions can be different and can affect the benefits of managing interfraction variations. In a separate study, we are investigating the differences of intrafraction motion between the left and supine postions [24]. The preliminary data showed that the intrafraction motion for left decubitus was not worse than that for the supine position. In addition, we are working with an immobilization device vendor to design robust customizable immobilization methods to improve patient comfortability, thus, increasing positioning stability and set up reproducibility while reducing intrafraction motion. Another concern is that inter-fractional positioning reproducibility may be reduced from the supine to the left decubitus. However, the online adaptive replanning that is often performed for each treatment fraction in MRgRT eliminates this concern. With improved immobilization techniques, the left decubitus

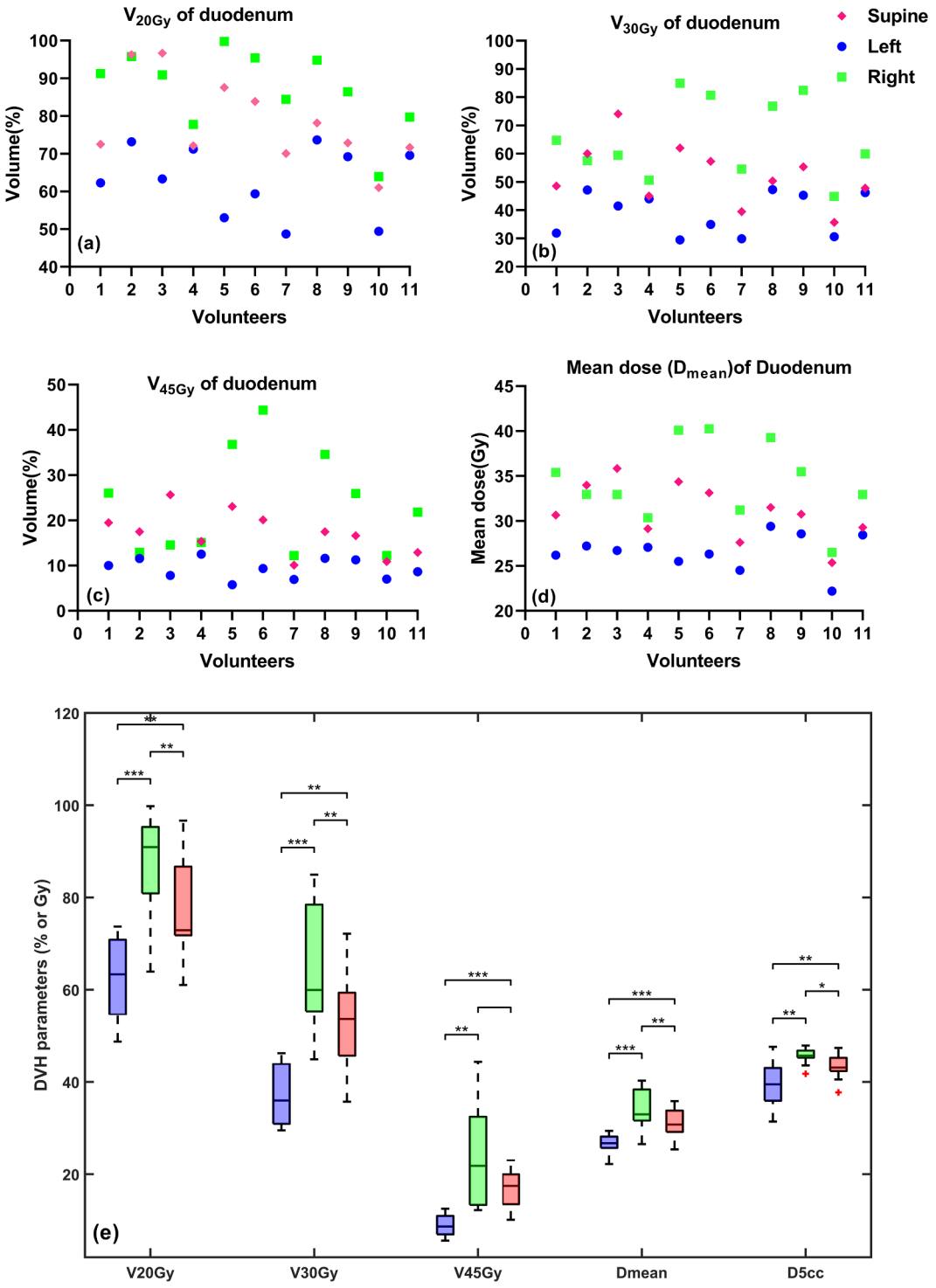

Fig. 3. A comparison of selected dose-volume parameters of duodenum for the supine, left, and right decubitus for all 11 cases studied. The values of V_{20Gy}, V_{30Gy}, V_{45Gy}, and D_{mean} are in shown in panel (a), (b), (c) and (d), While the box plots in (e) show the statistic differences of V_{20Gy}, V_{30Gy}, V_{45Gy}, D_{mean}, and D_{5cc} between the three positions. The symbols '*', '**' and '***' represent $P < 0.05$, 0.01, 0.001, respectively, based on the paired *t*-test of every two decubitus positions.

positioning may also be used for treatments on regular linac.

The study shows that the left decubitus leads to increased separation between pancreatic head and duodenum, resulting in improved sparing of duodenum during RT for pancreatic cancer. The use of the left decubitus positioning does not necessarily affect RT workflow. With a custom-made immobilization device, CT and/or MRI based planning images may be acquired for patient in the left decubitus position with the immobilization device during RT simulation. The data presented were collected from healthy volunteers. The clinical feasibility for the decubitus needs to be tested on patients.

5. Conclusions

The results indicate that the left decubitus in radiation therapy for pancreatic cancer leads to increased separation between pancreatic head and duodenum, which results in improved sparing of OARs,

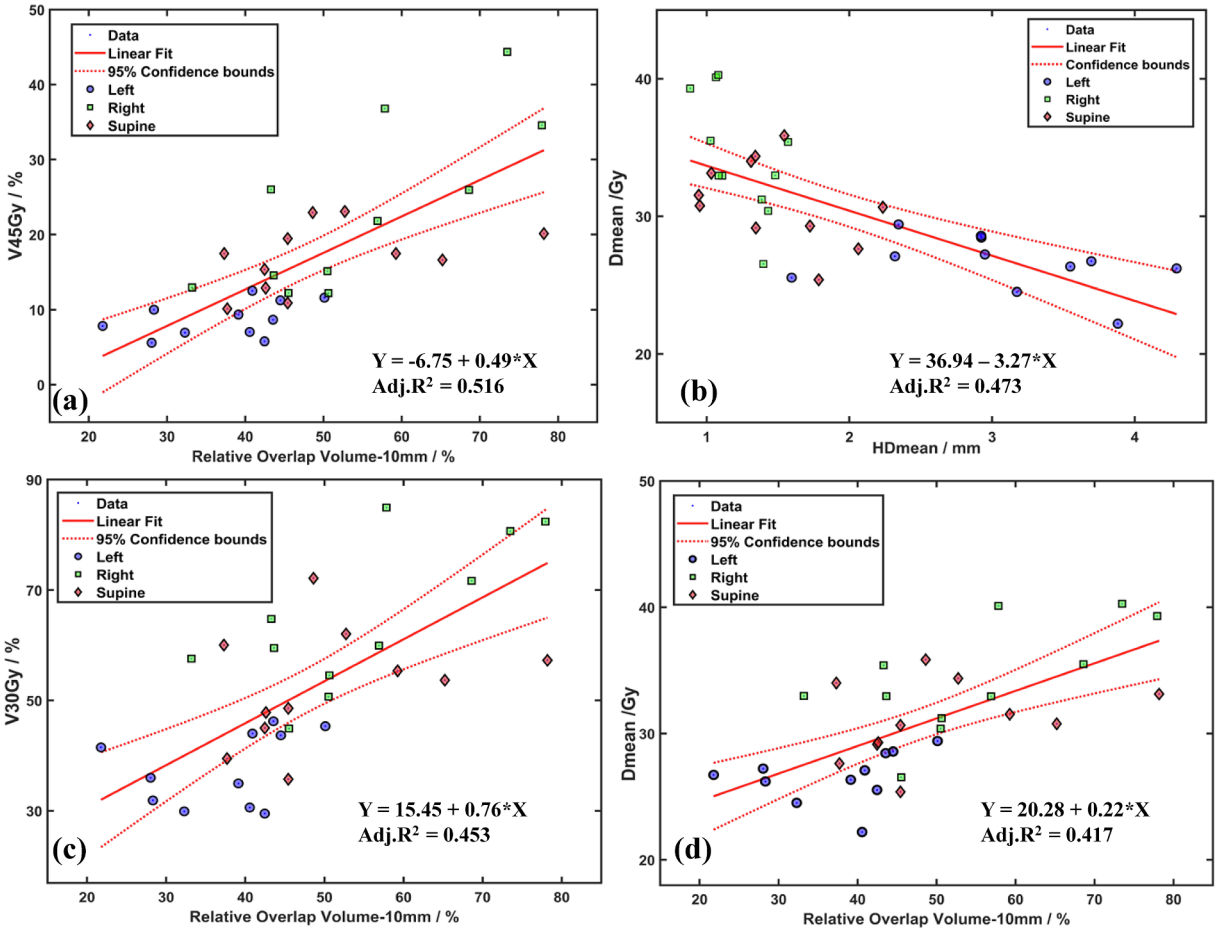

Fig. 4. Linear fitting of four highest correlated geometry and dosimetry parameters pairs for the pancreatic head and duodenum, including (a) ROV_{10mm} vs V_{45Gy}, (b) HD_{mean} vs D_{mean}, (c) ROV_{10mm} vs V_{30Gy}, and (d) ROV_{10mm} vs D_{mean}. Here ROV_{10mm} is the ratio of overlap volume between a 10 mm outer shell around pancreatic head contour and the duodenum to the duodenum volume. The obtained formula and Adjust R2 value were included in each figure. The ring, diamond, rectangle symbols represent data from left, supine, right decubitus, respectively.

allowing safer dose escalations to the tumors. The left decubitus positioning with proper immobilization can be feasible for MRI guided RT.

Declaration of Competing Interest

The authors declare that they have no known competing financial interests or personal relationships that could have appeared to influence the work reported in this paper.

Acknowledgements

This work was partially supported by Elekta AB, Stockholm, Sweden, by MCW Meinerz Foundation, and by Key project of Health Commission of Sichuan Province, 18ZD049. Constructive discussion with Sarah Hoffe, MD, is appreciated.

Appendix A. Supplementary data

Supplementary data to this article can be found online at https://doi.org/10.1016/j.phro.2019.11.001.

References

[1] Garrido-Laguna I, Hidalgo M. Pancreatic cancer: from state-of-the-art treatments to promising novel therapies. Nat Rev Clin Oncol 2015;12(319). https://doi.org/10.1038/nrclinonc.2015.53.

[2] Hammel P, Huguet F, van Laethem J, et al. Effect of chemoradiotherapy vs chemotherapy on survival in patients with locally advanced pancreatic cancer controlled after 4 months of gemcitabine with or without erlotinib: The lap07 randomized clinical trial. JAMA 2016;315(1844–53). https://doi.org/10.1001/jama.2016.4324.

[3] Landau E, Kalnicki S. The Evolving role of radiation in pancreatic cancer. Surg Clin 2018;98(113–25). https://doi.org/10.1016/j.suc.2017.09.008.

[4] Hall WA, Colbert LE, Nickleach D, Switchenko J, Liu Y, Gillespie T, et al. The influence of radiation therapy dose escalation on overall survival in unresectable pancreatic adenocarcinoma. J Gastrointest Oncol 2014;5(77–85). https://doi.org/10.3978/j.issn.2078-6891.2014.001.

[5] Lagendijk JJ, Raaymakers BW, van Vulpen M. The magnetic resonance imaging-linac system. Semin Radiat Oncol 2014;24(207–9). https://doi.org/10.1016/j.semradonc.2014.02.009.

[6] Acharya S, Fischer-Valuck BW, Kashani R, Parikh P, Yang D, Zhao T, et al. Online magnetic resonance image guided adaptive radiation therapy: first clinical applications. Int J of Radiat Oncol Biol Phys 2016;94:394–403. https://doi.org/10.1016/j.ijrobp.2015.10.015.

[7] Chen X, Prior P, Chen GP, Schultz CJ, Li XA. Dose effects of 1.5 T transverse magnetic field on tissue interfaces in MRI-guided radiotherapy. Med Phys 2016;43:4797–802.

[8] Ates O, Ahunbay EE, Moreau M, Li XA. A fast online adaptive replanning method for VMAT using flattening filter free beams. Med Phys 2016;43:2756–64.

[9] Rudra S, Jiang N, Rosenberg SA, Olsen JR, Roach MC, Wan L, et al. Using adaptive magnetic resonance image-guided radiation therapy for treatment of inoperable pancreatic cancer. Cancer Med 2019. https://doi.org/10.1002/cam4.2100.

[10] El-Bared N, Portelance L, Spieler BO, Kwon D, Padgett KR, Brown KM, et al. Dosimetric benefits and practical pitfalls of daily online adaptive MRI-guided stereotactic radiation therapy for pancreatic cancer. Pract Radiat Oncol 2019;9:e46–54. https://doi.org/10.1016/j.prro.2018.08.010.

[11] Bohoudi O, Bruynzeel AME, Senan S, Cuijpers JP, Slotman BJ, Lagerwaard FJ, et al. Fast and robust online adaptive planning in stereotactic MR-guided adaptive radiation therapy (SMART) for pancreatic cancer. Radiother Oncol

2017;125(439–44). https://doi.org/10.1016/j.radonc.2017.07.028.
[12] Henke L, Kashani R, Robinson C, Curcuru A, DeWees T, Bradley J, et al. Phase I trial of stereotactic MR-guided online adaptive radiation therapy (SMART) for the treatment of oligometastatic or unresectable primary malignancies of the abdomen. Radiother Oncol 2018;126(519–26). https://doi.org/10.1016/j.radonc.2017.11.032.
[13] Henke LE, Contreras JA, Green OL, Cai B, Kim H, Roach MC, et al. Magnetic resonance image-guided radiotherapy (MRIgRT): A 4.5-year clinical experience. Clin Oncol (R Coll Radiol) 2018;30(720–7). https://doi.org/10.1016/j.clon.2018.08.010.
[14] Takatsu Y, Akasaka T, Miyati T. The Dixon technique and the frequency-selective fat suppression technique in three-dimensional T1 weighted MRI of the liver: a comparison of contrast-to-noise ratios of hepatocellular carcinomas-to-liver. BJR 2015;88(20150117). https://doi.org/10.1259/bjr.20150117.
[15] Drukker K. Applied Medical Image Processing, Second Edition: A Basic Course. SPIE; 2014. p. 2.
[16] Karotki A, Mah K, Meijer G, Meltsner M. Comparison of bulk electron density and voxel-based electron density treatment planning. J Appl Clin Med Phys 2011;12:97–104. https://doi.org/10.1120/jacmp.v12i4.3522.
[17] Prior P, Chen X, Botros M, Paulson ES, Lawton C, Erickson B, et al. MRI-based IMRT planning for MR-linac: comparison between CT- and MRI-based plans for pancreatic and prostate cancers. Phys Med Biol 2016;61(3819–42). https://doi.org/10.1088/0031-9155/61/10/3819.
[18] Prior P, Chen X, Gore E, Johnstone C, Li XA. Technical Note: Is bulk electron density assignment appropriate for MRI-only based treatment planning for lung cancer? Med Phys 2017;44(3437–43). https://doi.org/10.1002/mp.12267.
[19] Chung SY, Chang JS, Lee BM, Kim KH, Lee KJ, Seong J. Dose escalation in locally advanced pancreatic cancer patients receiving chemoradiotherapy. Radiother Oncol 2017;123(438–45). https://doi.org/10.1016/j.radonc.2017.04.010.
[20] Krishnan S, Chadha AS, Suh Y, Chen HC, Rao A, Das P, et al. Focal Radiation therapy dose escalation improves overall survival in locally advanced pancreatic cancer patients receiving induction chemotherapy and consolidative chemoradiation. Int J Radiat Oncol Biol Phys 2016;94(755–65). https://doi.org/10.1016/j.ijrobp.2015.12.003.
[21] Zaorsky NG, Lehrer EJ, Handorf E, Meyer JE. Dose escalation in stereotactic body radiation therapy for pancreatic cancer: a meta-analysis. Am J Clin Oncol 2018. https://doi.org/10.1097/coc.0000000000000472.
[22] Badiyan SN, Olsen JR, Lee AY, Yano M, Menias CO, Khwaja S, et al. Induction chemotherapy followed by concurrent full-dose gemcitabine and intensity-modulated radiation therapy for borderline resectable and locally advanced pancreatic adenocarcinoma. Am J Clin Oncol 2016;39(1–7). https://doi.org/10.1097/coc.0000000000000003.
[23] Moraru IC, Tai A, Erickson B, Li XA. Radiation dose responses for chemoradiation therapy of pancreatic cancer: An analysis of compiled clinical data using biophysical models. Pract Radiat Oncol 2014;4:13–9. https://doi.org/10.1016/j.prro.2013.01.005.
[24] Wang L, Keiper T, Chen X, Erickson B, Li XA, Intrafractional motions in three decubitus body decubitus positions for radiation therapy of pancreatic cancer. ASTRO annual meeting, Chicago, 2019 (abs).